Proceedings of ASME Turbo Expo 2017: Turbomachinery Technical Conference and Exposition
GT2017
June 26-30, 2017, Charlotte, NC, USA

GT2017-64055

FUEL UTILIZATION EFFECTS ON SYSTEM EFFICIENCY AND SOLID OXIDE FUEL CELL PERFORMANCE IN GAS TURBINE HYBRID SYSTEMS

Nor Farida Harun*, Lawrence Shadle, Dan Oryschyn, David Tucker
U.S. Department of Energy
National Energy Technology Laboratory
U.S.A

ABSTRACT

The simulation work presented herein characterizes the performance of a recuperated gas turbine (GT) hybrid systems in response to different levels of fuel utilization (U_f) by the SOFC. The SOFC performance was compared with and without anode recycle (AR), operating at 90% total stack U_f ($U_{f.stack}$). A study at 65% U_f was also considered as a reference case for the hybrid power system without anode recycle, i.e. using single-pass cell fuel utilization ($U_{f.cell}$). All three cases in this paper were evaluated at design points for a 550 MW hybrid system using coal-derived syngas feed with zero methane.

A previously developed one-dimensional (1D) fuel cell model was used to simulate the distributed profile of thermal and electrochemical properties along the fuel cell length. Fuel cell total current density, average solid temperature, and cathode inlet temperature were maintained identical at each fuel utilization to avoid confounding the results with the impacts of SOFC degradation.

The maximum system efficiency of 71.1% was achieved by SOFC/GT non-recycle systems at 90% $U_{f.cell}$ (with 90% $U_{f.stack}$). The case at 65% $U_{f.cell}$ (with 65% $U_{f.stack}$) demonstrated 70.7% total efficiency, only 0.4% point lower than at 90% $U_{f.cell}$. However, integrating anode recycle to the system significantly reduced the maximum total efficiency to 55.5%. Although the distributed SOFC performance across the cell length for 65% $U_{f.cell}$ with AR at 90% $U_{f.stack}$ was similar to the 65% $U_{f.cell}$ (with 65% $U_{f.stack}$), recycling anode off-gas resulted in lower fuel cell Nernst potential that caused further drop in both stack and total system efficiency.

Keyword: hybrid efficiency; fuel utilization; solid oxide fuel cell gas turbine hybrid; anode recycle

INTRODUCTION

Fuel utilization is one of the key variables determining solid oxide fuel cell (SOFC) system efficiency and usable SOFC lifetime, both of which are associated with plant economics. Fuel utilization (U_f) is commonly defined as the ratio of fuel consumption to the fuel feed for electrochemical power generation. Intuitively, SOFC efficiency continuously increases with increasing fuel utilization [1, 2]. However, the SOFC performance is also a strong function of temperature, current density, and voltage [1-4]. As such, the selection of fuel utilization for maximum efficiency is strongly coupled to major SOFC operating conditions, as well as the stack design [5].

Operating state-of-the-art fuel cells at high fuel utilization is required in standalone SOFC systems to achieve high system efficiency. Such SOFCs are expected to operate as much as 90% U_f because of their sole dependence on SOFC power generation [6]. However, operating the SOFC systems at high fuel utilization in a conventional single-pass flow is very challenging due to greater degradation risk, corresponding to uneven local fuel distribution over the cell active area [7, 8]. Depletion of H_2 at high fuel utilization in the cell can lead to the oxidation of anode material [9, 10]. Consequently, this degradation mechanism reduces the catalytic activity, the cell active area, and increases the polarization losses [11]. The cells can degrade much faster if running them at higher current density to compensate for the voltage loss over time. The result is more rapid degradation rates [12].

Recycling part of the anode-off gas back to the SOFC anode inlet is one common solution to achieve high system efficiency while using the low single-pass cell fuel utilization required for standalone SOFC configurations [13]. Previous studies show that it is possible to increase the electrical efficiency as much as 16% in SOFC system alone using anode recycle [14, 15]. However, the system SOFC efficiency varies, depending on the recirculation ratio, the single-pass cell fuel

*This work was done under the U.S. Department of Energy (DOE) Postgraduate and Graduate Research Program at the National Energy Technology Laboratory (NETL), managed by the Oak Ridge Institute for Science and Education (ORISE)

utilization, the resulting parasitic power from the blower, ejector, or pump in the recycling operations, and other critical SOFC performance variables [15, 16]. Thus, the challenges in system controllability also increase, especially for part-load operations [13, 15].

SOFC gas turbine (SOFC/GT) hybrid systems offer a viable solution to extending the fuel cell life while maintaining relatively high efficiencies. These are achievable by operating the fuel cells at lower fuel utilization [17]. Due to load sharing capability between the SOFC and the gas turbine in SOFC/GT hybrid systems, the unutilized fuel from the stack and the high temperature cathode-off gas are efficiently recovered in the gas turbine for additional power production. As such, the total hybrid system efficiency is less sensitive to the SOFC fuel utilization [17-19]. In addition, decreasing the SOFC fuel utilization in the hybrid systems under high system operating pressure improves the Nernst potential and could possibly extend the fuel cell life [12,17].

As the total hybrid system efficiency is not mainly driven by high SOFC fuel utilization, anode recycle in hybrid systems are not as critical as in standalone SOFC systems. In fact, the use of anode recycle in the hybrid systems is expected to cause more problematic control issues because of the highly coupled behavior in the hybrid configurations. However, the effects of anode recycle on the SOFC distributed electrochemical performance in GT hybrid performance are not clearly discussed [1, 19].

Previous SOFC/GT analyses commonly use 85% U_f SOFC to evaluate the hybrid performance for various purposes, assuming that maximizing the power output from the SOFC leads to the highest possible efficiency [20]. For instance, the studies included an optimization of compressor and turbine design in a hybrid configuration [21], thermoeconomic analysis comparing atmospheric and pressurized hybrid systems [22], design analysis of SOFC/GT hybrid cycles using H_2 fuel [1], controls [23, 24], and system performance of SOFC intercooled gas turbine cycle [25].

Operating the SOFC at 70% U_f, 80% U_f, and 85% U_f were also considered in an analysis of SOFC/GT hybrid and integrated gasification fuel cell turbine (IGFC) systems [26]. In summary, the range of fuel utilization in hybrid systems found in the literature varied approximately between 50% U_f and 90% U_f [1, 18, 20]. However, the actual relationship between fuel utilization and the system efficiency at the design operating conditions were not tested. In addition, the influence of the fuel utilization on the power system were missing and could not be assessed because the simulation studies used overly simplified lumped SOFC models.

Motivated by the aforementioned gaps, this work was undertaken to better understand the relationship between the SOFC fuel utilization and the SOFC/GT hybrid efficiency within the design points for a 550MW power plant relevant to centralized power production. Different SOFC stack, compressor, and gas turbine sizes were considered to match up the desired total hybrid power. The analysis presented herein focuses around the following major contributions:

1) The effects of fuel utilization on the SOFC/GT hybrid system efficiency were investigated using a traditional single-pass (non-recycle) configuration. For this case, the total stack U_f ($U_{f.stack}$) was the same as the cell system U_f ($U_{f.cell}$). The system performance at 65% $U_{f.cell}$ (low fuel utilization) was compared with that at 90% $U_{f.cell}$ (high fuel utilization).
2) The contribution of anode recycle was investigated at 65% $U_{f.cell}$ (with 90% $U_{f.stack}$) and compared to non-recycle systems at 90% $U_{f.cell}$ (with 90% $U_{f.stack}$) and 65% $U_{f.cell}$ (with 65% $U_{f.stack}$).
3) In this study, the SOFC electrical performance was evaluated based on the distributed SOFC profiles across the cell length. A one-dimensional (1D) SOFC model was used to determine local current density, fuel utilization, temperature profiles, and polarization losses. As such, the coupling of each critical SOFC variable and its influence in determining the system efficiency could be studied.
4) This analysis considered coal-derived syngas with zero methane as the SOFC fuel rather than a traditional fuel, H_2, due to more flexible and more economical fuel options for advanced power generation systems [12, 19, 27]. The fuel composition is expected to have a more significant influence on the hybrid system performance as compared to that of the standalone SOFC due to the potential for post-combustion of the anode-off gas to recover the heating value with the gas turbine cycle.

All cases were studied at a constant total fuel cell current, a constant cathode inlet temperature, and a fairly constant average SOFC temperature to minimize variation in the temperature gradient across the fuel cell. A hot air bypass valve was employed to regulate cathode inlet air mass flow at lower fuel utilization in order to maintain a fixed cathode inlet temperature.

METHODOLOGY

System Configuration of SOFC/GT Hybrid System

A solid oxide fuel cell gas turbine (SOFC/GT) hybrid system in a recuperated configuration shown in Fig. 1 was used for the analysis presented in this paper. Fuel fed into SOFC anode was the only fuel source for power generation in the hybrid system. Complete fuel oxidation occurred in a post-combustor with the high quality cathode-off gas from the high temperature SOFC. The hot gases from the post-combustor were eventually expanded across the turbine to generate power to supplement the SOFC power. In this system, cathode inlet air was compressed and then pre-heated by a gas turbine recuperation system to achieve the desired SOFC operating conditions before entering the stack. A secondary method of heat exchange also occurred at the cathode inlet upstream, which resulted from the heat exchange in the fuel cell air manifold systems.

If the exhaust gas turbine temperature was too high for heat recuperation systems due to high anode-off gas fuel flow resulting from low fuel utilization operations, the cathode inlet temperature could exceed the tolerable limit. One practical solution for this problem was bypassing the compressed air flow after the recuperation unit to the post-combustor inlet through a hot air bypass valve. This bypass strategy relaxed the constraint on both post combustor and turbine inlet temperature.

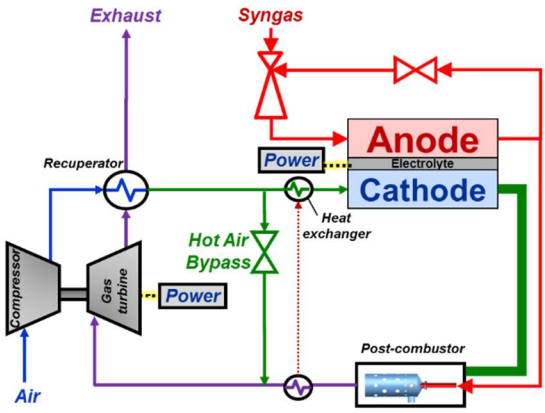

Figure 1: Recuperated SOFC/GT hybrid system

One-Dimensional Solid Oxide Fuel Cell Model

In this study, a previously developed one dimensional (1D) fuel cell model was used to simulate the distributed performance of SOFC in the hybrid system. The model was developed in MATLAB Simulink environment for a planar, co-flow, and anode-supported SOFC configuration. A standard material using 441 stainless steel was considered for interconnects, while nickel-doped yttria-stabilized zirconia (Ni-YSZ), YSZ- lanthanum strontium magnetite (LSM), and YSZ were used as anode, cathode, and electrolyte, respectively. A temperature range of 300 K to 1800 K was selected to estimate the temperature-dependent thermophysical properties of each material used in the model. This model was successfully validated and verified against three sets of simulation results provided by IEA benchmarking data sets, and other simulation studies [28-30]. The detailed work of the model development was discussed in a previous publication [28].

The 1D fuel cell model was able to simulate the main fuel cell thermal and electrochemical process variables as a function of time at 20 local positions or nodes across the fuel cell length. A 20 cm fuel cell was discretized into 20 nodes with a length of 1 cm each. Conductive heat transfer in solid materials, convective heat transfer between solid components and gas stream in the system, and heat generation resulting from electrochemical reaction, water-gas shift, and steam methane reforming, were considered as heat transfer mechanisms in the model. The SOFC model was also simplified as follows:

1. H_2 was the only active species for electrochemical oxidation. Direct electrochemical oxidation of CO and CH_4 were assumed to be negligible because the kinetics of CO and CH_4 electrochemical oxidation were relatively slow compared to H_2 oxidation, limited surface area was available for electrochemical oxidation, and the cases simulated in this paper were only with excess water concentrations.
2. All electrochemical properties were temperature-dependent variables, which responded to distributed temperature profiles.
3. Fuel cell performance was evaluated as a single cell, and the stack performance was calculated by simply multiplying by the total cell numbers.
4. A fuel processing unit was not considered. As such, fuel feed was supplied at the desired SOFC operating temperature and pressure.
5. No pressure loss across the fuel cell.
6. Heat loss to the surrounding was neglected.
7. Complete fuel oxidation in the combustor systems.
8. Dissociation in combustion was neglected due to low combustion temperatures.

To date, the same model was applied to investigate fuel cell performance at various transient events, including during electrochemical light-off [31], thermal management using control bypass valves [32, 33], SOFC fuel composition transitions [34], and accelerated SOFC degradation [35]. However, the work discussed in this paper particularly implemented the 1D fuel cell model for steady state performance analysis.

As shown in Fig. 2, the single-pass cell fuel utilization ($U_{f.cell}$) and total stack fuel utilization ($U_{f.stack}$) in this work were defined based on hydrogen consumption. The calculation for $U_{f.cell}$ and $U_{f.stack}$ were summarized in Eq. (1) and (2) respectively.

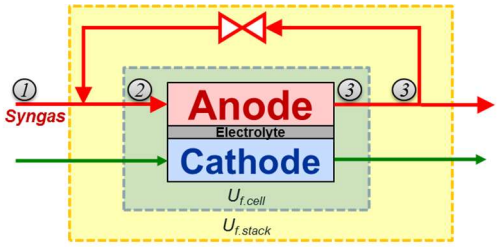

Figure 2: SOFC boundary for fuel utilization calculation

Single-pass cell utilization:

$$U_{f.cell} = 1 - \frac{x_{H_2}(at\ point\ 3)}{x_{H_2}(at\ point\ 2)} \qquad (Eq.1)$$

Total stack fuel utilization:

$$U_{f.stack} = 1 - \frac{x_{H_2}(at\ point\ 3)}{x_{H_2}(at\ point\ 1)} \qquad (Eq.2)$$

Note that if anode recycle was not considered, hydrogen composition, x_{H_2}, at point 2 was equivalent to that at point 1.

Therefore, $U_{f.cell}$ and $U_{f.stack}$ were the same. In the case with anode recycle, $U_{f.stack}$ was greater than $U_{f.cell}$ for the same total current and main fuel supply flow rate.

Localized fuel utilization ($U_{f.node}$) was applied at each node as described by Eq. (3), where *n* represents a current node and *n+1* represents the following node. Note that mole fraction of the components, x_i, used in all fuel utilization calculations was resolved at node level.

$$U_{f.node}(n) = 1 - \frac{x_{H_2}(n+1) + x_{CO}(n+1) + 4x_{CH_4}(n+1)}{x_{H_2}(n) + x_{CO}(n) + 4x_{CH_4}(n)} \quad (Eq.3)$$

The cell voltage, V_{cell}, was quantified using an expression in Eq. (4) based on Nernst potential, V_{Nernst}, or open circuit potential. The cell voltage was reduced from Nernst potential expressed in Eq. (5) because of the irreversible losses: diffusion loss, η_{dif}, activation loss, η_{act},and ohmic loss, η_{ohm}, which are presented in Eq. (6), (7), and (8), respectively. As indicated in Eq. (4) to Eq. (8), all voltage, Nernst potential, and electrochemical losses changed in response to variations in composition and temperature distribution. The exchange current density, i_0, for both cathode and anode sides was also dependent on temperature profiles. *TBP* in Eq. (6) denotes the triple-phase boundary layer. The distributed performance of current density, Nernst potential, and electrochemical losses were resolved for each node, assuming uniform voltage over the cell.

$$V_{cell} = V_{Nernst} - \eta_{dif} - \eta_{act} - \eta_{ohm} \quad (Eq.4)$$

$$V_{Nernst} = -\frac{\Delta G^{\circ}_{H_2O}}{2F} + \frac{R_u T}{2F} ln\left[\frac{p_{H_2}.p_{O_2}^{0.5}}{p_{H_2O}}\right] \quad (Eq.5)$$

$$\eta_{dif} = \frac{R_u T}{2F}\left(\ln\left(\frac{x_{H_2,bulk}.x_{H_2O,TBP}}{x_{H_2O,bulk}.x_{H_2,TBP}}\right) + \frac{1}{2}\ln\left(\frac{x_{O_2,bulk}}{x_{O_2,TBP}}\right)\right) \quad (Eq.6)$$

$$\eta_{act} = \frac{R_u T}{\alpha n F}\sinh^{-1}\left(\frac{i}{2i_0}\right) \quad (Eq.7)$$

$$\eta_{ohm} = ASR \cdot i \quad (Eq.8)$$

An empirical model for localized cell degradation rate as shown in Eq. (9) was also included in the analysis. Eq. (9) demonstrates that the cell degradation rate was a function of fuel utilization, U_f, solid temperature, *T*, and current density, *i*, calculated at each node to evaluate the percentage of voltage drop in 1000 hours across the fuel cell length.

$$r_d = \frac{0.59U_f + 0.74}{1 + \exp\left(\frac{T - 1087}{22.92}\right)}\left(e^{2.64i} - 1\right) \quad (Eq.9)$$

The correlation in Eq. (9) was developed based on a curve fitting method using experimental data obtained from two different physical SOFC test units, one located at the National Energy Technology Laboratory, and one at the Denmark Technical University [35]. The experiments measured voltage versus time for different current density and fuel utilizations at various operating temperatures using the same sets of material and fuel composition. The effect of impurities and pressure were not included in the development of this empirical expression. The localized cell degradation rate in this work was estimated using the final steady state values.

Simulation Strategy and Analysis

An integration of a 1D fuel cell model and a recuperated gas turbine cycle model was adopted for steady state SOFC/GT cycle analysis. A total power generation of 550 MW was selected as a target size for demonstration of potential future market entry. In this study, the number of cells in the fuel cell stacks was varied as a design parameter along with compressor and turbine sizes to bring the SOFC system to the desired fuel utilization for a 550 MW total hybrid power generation. Therefore, the model predicted SOFC distributed performance at different design points for the hybrid cycle. Fixed and variable hybrid operating parameters used in the simulations are summarized in Table 1 and Table 2.

The model simulated three main cases using the same SOFC materials and configuration, as listed in Table 1. The first and the second cases were both for a system without anode recycle (AR), operating at 90% $U_{f.cell}$ (90% $U_{f.stack}$) and 65% $U_{f.cell}$ (65% $U_{f.stack}$). Meanwhile, the third case was for a system with AR at 65% $U_{f.cell}$ (90% $U_{f.stack}$). It was assumed that 65% $U_{f.cell}$ was an optimized value for a trade-off between SOFC performance, efficiency and economic benefits. As such, all three simulations were compared to evaluate the influence of fuel utilization on the efficiency and the effects of anode recycle.

Although the results presented herein were collected from simulations of an entire gas turbine hybrid cycle, the main discussion and analysis in this paper was limited to SOFC performance as a subsystem of SOFC/GT hybrid. The detailed investigation of the hybrid system performance at the design points related to this study will be published in a separate work.

Table 1 Fixed SOFC/GT hybrid operating parameters

SOFC system parameters	
Current density	550 mA/cm^2
Initial fuel cell temperature	1073 K
Cathode inlet pressure	405 kPa
Cathode inlet temperature	973 K
Fuel cell average solid temperature	1108 K
Cathode inlet composition (mole fraction): Air	21% O_2, 79% N_2
Anode inlet pressure	405 kPa
Main fuel supply temperature	1073 K
Main fuel supply composition (mole fraction): coal-derived syngas	CH_4 0%, CO_2 12.0%, CO 28.6%, H_2 29.1%, H_2O 27.1%, N_2 3.2%
SOFC Geometry	
Total cell area	200 mm x 200 mm

Anode thickness	0.5 mm
Electrolyte thickness	0.008 mm
Cathode thickness	0.05 mm
Oxidant/fuel channel size	2 mm x 2 mm
Number of oxidant/fuel channels	50
Number of fuel cell nodes	20 (1 cm each)
GT system parameters	
Pressure Ratio	4
Compressor isentropic efficiency	83.6 %
Gas turbine isentropic efficiency	87.0%
Recuperator parameters	
Effectiveness of gas turbine recuperation system	93.0%
Pressure drop	
Cold side pressure drop in gas turbine recuperation system	4.0%
Hot side pressure drop in gas turbine recuperation system	6.0%
Total system pressure drop (i.e. bypass valve is closed)	8.0%
Minimum total system pressure drop	2%

Table 2 Variable SOFC/GT hybrid operating conditions

Fuel utilization	0.65 – 0.90
Oxygen utilization	0.00 – 0.17
Anode recycle, AR	0 – 100 %
Hot air bypass	0 – 100%

Cathode air mass flows was varied in all simulations, depending on the stack requirement at a specified fuel utilization. The cathode air flow was regulated such that oxygen utilization was maintained lower than 17% to ensure excess air conditions while maintaining sufficient energy to preheat the air. A hot air bypass valve (Fig. 1) was used to manage cathode inlet air mass flow at a lower fuel utilization. Air flow bypass was important to meet the limited turbine operating conditions and to get a constant cathode inlet temperature of 973 K. As a result of high sensible heat in the post combustor outlet stream due to increased unutilized fuel, the system operated at 65% $U_{f.cell}$ (65% $U_{f.stack}$) required 31.5% hot air bypass.

To represent the heat exchange occurring in the SOFC air manifold system, a low effectiveness heat exchanger between the cathode inlet and the post-combustor outlet was considered in the simulation work (Fig. 1). The range of the effectiveness was varied in order to achieve a 973 K cathode inlet temperature. For the case with 65% $U_{f.cell}$ (65% $U_{f.stack}$), a very lower effectiveness (0.0006) was used due to higher SOFC thermal output. In contrast, both cases with 90% $U_{f.stack}$ required higher effectiveness (0.38 to 0.48) and 0% hot air bypass to provide enough pre-heating energy.

Average solid temperature also changed, following the cathode air mass flow variations. Thus, the average solid temperature in each simulation was maintained approximately constant at 1108 K with a delta solid temperature between the inlet and outlet lower than 125 K. The limiting temperature strategy was essential to minimize the coupling effects of cathode air mass flow on temperature gradient across the fuel cell length. The SOFC model was run using the variable input parameters, considering various operating limits and system targets simultaneously.

RESULTS AND DISCUSSION

The localized fuel utilization across the fuel cell is shown in Fig. 3. The localized U_f for 65% $U_{f.cell}$ (90% $U_{f.stack}$) and 65% $U_{f.cell}$ (65% $U_{f.stack}$) were nearly coincident, while the 90% $U_{f.cell}$ (90% $U_{f.stack}$) were much higher in all nodes across the fuel cell. The SOFC system in all case studies generated a maximum H_2 partial pressure between node 1 and node 2 as the water-gas shifting was dominating (Fig. 4). As a consequence, CO within the same region decreased dramatically (Fig. 5). However, the fuel utilization between node 1 and node 2 as shown in Fig. 3 still increased because the H_2 consumption in electrochemical oxidation was greater than its formation due to water-gas shifting process.

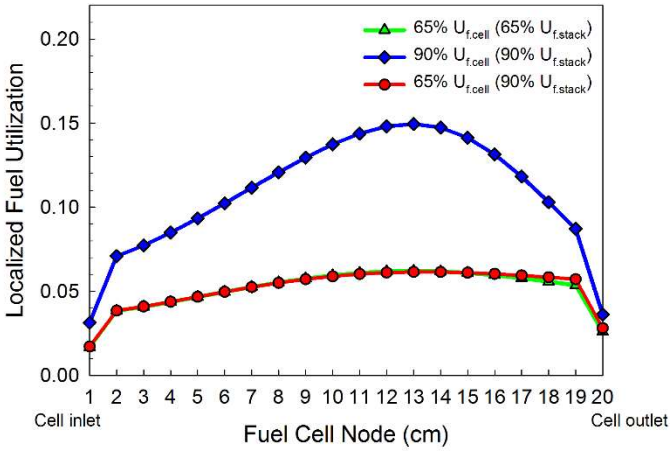

Figure 3: Localized fuel utilization, $U_{f.node}$

In addition to the availability in the fuel feed, the net H_2 presence was driven by water-gas shifting equilibrium and electrochemical oxidation, which are defined in Eq. (10) to Eq. (12). In contrast, CO content was solely dependent on water-gas shifting equilibrium because methane was not available in the fuel feed to drive steam-methane reforming. Therefore, as shown in Fig. 5, CO continually decreased along the fuel cell length as the shift reaction favored the H_2 and CO_2. Note that the water-gas shift reaction was assumed to be at equilibrium in the selected temperature range.

Water-gas shifting:

$$CO + H_2O \rightleftharpoons H_2 + CO_2 \quad \left(\Delta H^\circ = -41\frac{kJ}{mol}\right) \qquad (Eq.10)$$

$$K_{P,WGS} = \frac{P_{H_2}P_{CO_2}}{P_{H_2O}P_{CO}} = \frac{x_{H_2}x_{CO_2}}{x_{H_2O}x_{CO}} = exp\left[\frac{4276}{T} - 3.961\right] \qquad (Eq.11)$$

Hydrogen oxidation:

$$H_2 + \frac{1}{2}O_2 \rightarrow H_2O \qquad \left(\Delta H^\circ = -286\frac{kJ}{mol}\right) \qquad (Eq.12)$$

As expected, the local distribution of 65% $U_{f.cell}$ (90% $U_{f.stack}$) and 65% $U_{f.cell}$ (65% $U_{f.stack}$) were identical due to the same single-pass cell fuel utilization. As presented in Fig. 4 and 5, the partial pressure of H_2 and CO in 65% $U_{f.cell}$ (65% $U_{f.stack}$) were about 3 times higher than in the case of 65% $U_{f.cell}$ (90% $U_{f.stack}$). However, the rate of composition gradients across the cell for both cases were identical due the same cell performance as observed in the current density profiles shown in Fig. 6.

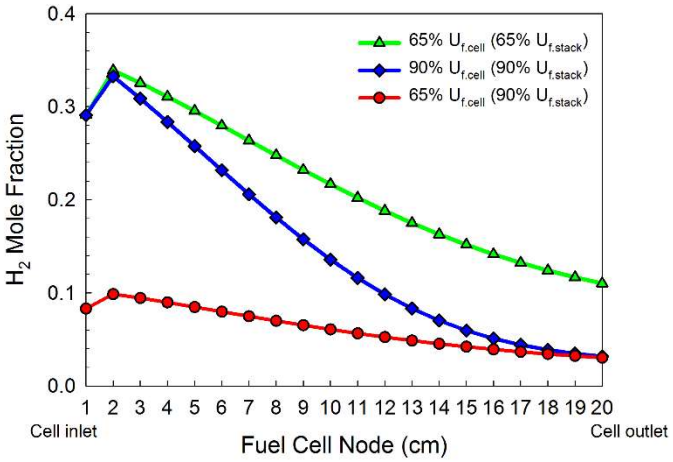

Figure 4: Distributed H_2 mole fraction

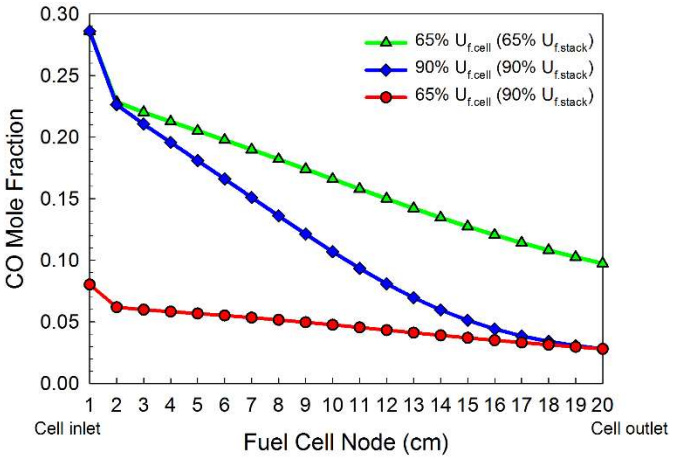

Figure 5: Distributed CO mole fraction

The distributed current density produced by 65% $U_{f.cell}$ (90% $U_{f.stack}$) in Fig. 6 closely followed the result of 65% $U_{f.cell}$ (65% $U_{f.stack}$), both of which demonstrated more evenly distributed fuel utilization (Fig. 3) in response to the current density performance. Although all cases were studied at a specified total current density of 550 mA/cm^2, the changes in current density across the cell for the 90% $U_{f.cell}$ (90% $U_{f.stack}$) were more remarkable.

Operating the SOFC system at 90% $U_{f.cell}$ (90% $U_{f.stack}$) resulted in increasing fuel utilization toward the cell outlet (Fig. 3). A local maximum of 15% fuel utilization was achieved at node 13 because of decreasing H_2 availability to this point, as shown in Fig. 4. However, the gradient in both H_2 and CO after node 13 became less significant. As there was less CO at lower H_2 partial pressure, the electrochemical oxidation decelerated, driving the shift reaction to use the CO to the lowest mole fraction at the cell exit.

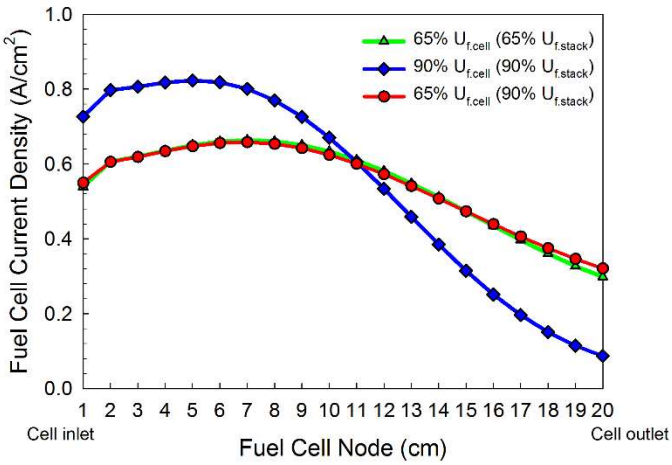

Figure 6: Localized current density

Fig. 3 to Fig. 6 clearly demonstrate the advantages of using the 1D fuel cell model with localized fuel cell performance. As opposed to a lump fuel cell model, the 1D model was able to capture the difference in composition gradient across the fuel cell length between the cases of 65% $U_{f.cell}$ (65% $U_{f.stack}$) and 65% $U_{f.cell}$ (90% $U_{f.stack}$), both were at the same $U_{f.cell}$. As such, the coupling between the fuel utilization with other fuel cell operating variables could be identified.

The distributed fuel cell solid and air temperature, as well as solid temperature gradient profiles are shown in Fig. 7 to Fig. 9. As shown in Fig. 7, the SOFC solid temperature increased to the maximum temperature at the outlet region. The solid temperature was leveling off after node 13, corresponding to reduced Nernst potential (Fig. 10) and current density (Fig. 6). The solid temperature in the last few nodes for the 65% $U_{f.cell}$ cases were higher than in 90% $U_{f.cell}$ because of higher current density as shown in Fig. 6.

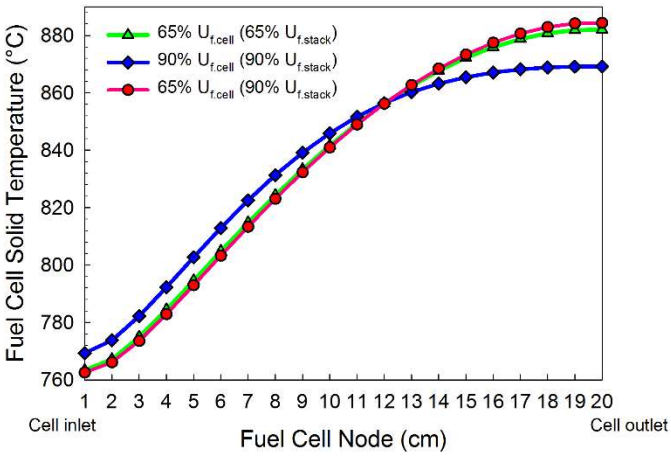

Figure 7: Fuel cell solid temperature

In general, the system featured similar variations in the SOFC thermal performance as a consequence of operating the SOFC/GT hybrid at a constant average SOFC temperature and cathode inlet gas temperature. However, 90% $U_{f.cell}$ (90% $U_{f.stack}$) showed a slightly different solid temperature profile since this case was run with approximately a 20 K lower delta solid temperature. The delta temperature obtained in each case is listed in Table 3.

Table 3 Selected SOFC variable parameters

Variable Parameters	65% $U_{f.cell}$ (65% $U_{f.stack}$)	90% $U_{f.cell}$ (90% $U_{f.stack}$)	65% $U_{f.cell}$ (90% $U_{f.stack}$)
Delta solid temperature, ($T_{solid\ out} - T_{solid\ in}$), K	119	100	122
O_2 utilization, %	17.0	14.6	14.3
Anode inlet flow, kg/s	101.2	100.3	128.8

Table 4 Size of SOFC/GT components

Fuel Utilization	Cathode air flow (kg/s)	Number of SOFC cells	Compressor air flow (kg/s)	Turbine power (MW)
65% $U_{f.cell}$ (65% $U_{f.stack}$)	797	1,694,000	1163	239.3
90% $U_{f.cell}$ (90% $U_{f.stack}$)	1270	2,325,000	1270	144.1
65% $U_{f.cell}$ (90% $U_{f.stack}$)	1252	2,240,000	1252	185.1

Operating the system at such a lower delta temperature eventually affected the solid temperature gradient across the fuel cell length as indicated in Fig. 8. However, substantial deviation in the temperature gradient only occurred in the downstream region after node 7. The SOFC thermal performance would have been identical if the delta solid temperature was also maintained approximately the same. Intuitively, the gradient in the SOFC solid temperature must be as minimal as possible to avoid thermal stress in the material.

In order to produce 550 MW total power from this hybrid system, different fuel utilization required different cathode air mass flow to maintain the desired temperature limits. As summarized in Table 4, the lowest fuel utilization, 65% $U_{f.cell}$ (65% $U_{f.stack}$), operated at the lowest cathode air flow requirement because as much as 30% pre-heated air flow intake was bypassed (Fig. 1). This was due to excessive temperature increase in the cathode inlet as more thermal energy provided into turbomachinery systems.

At higher fuel utilization, higher air mass flow was important for stack cooling but energy available through the recuperation unit to preheat the incoming compressed air flow was insufficient. Therefore, both operations at 90% $U_{f.stack}$ did not require any hot air bypass.

The corresponding changes in Nernst potential are shown in Fig. 10. As expressed in Eq. (5), the distributed profile of Nernst potential was strongly coupled with composition and SOFC solid temperature in each node. The trends of distributed Nernst potential across the fuel cell length qualitatively followed H_2 mole fraction gradient in Fig. 4.

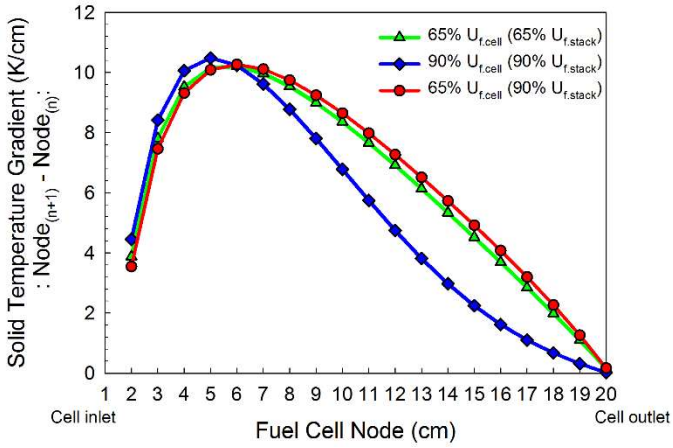

Figure 8: Fuel cell solid temperature gradient between each node.

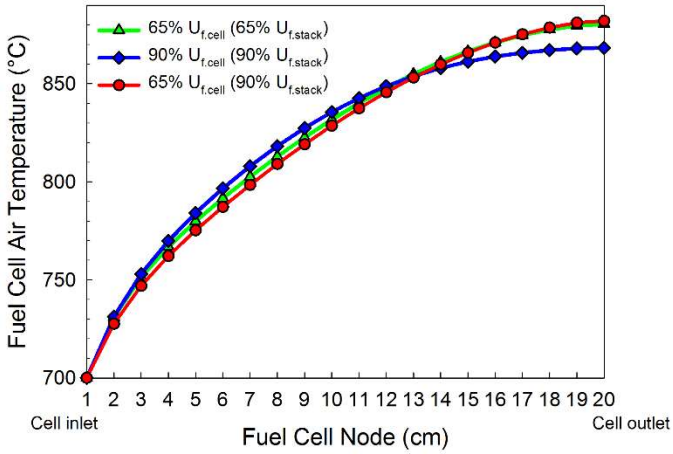

Figure 9: Fuel cell air temperature

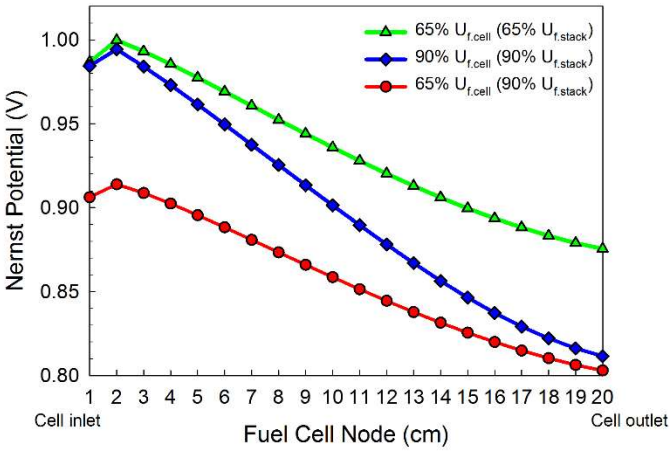

Figure 10: Localized Nernst potential

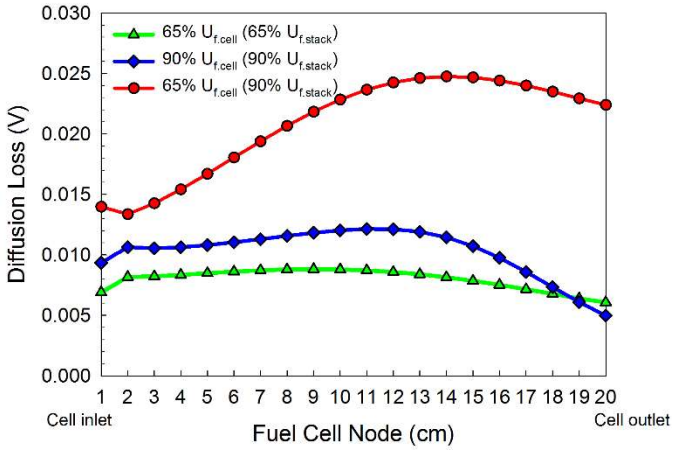

Figure 11: Localized diffusion loss

All operations studied in this paper demonstrated the maximum Nernst potential at the cell inlet region due to high H_2 content, as shown in Fig. 4. However, the Nernst potential started to deviate in the remaining cell length as the cell performance varied. The Nernst voltage in all cases decreased significantly toward the lowest potential at the cell exit due to the negative influence of H_2 depletion and high temperature in this region.

The non-recycle hybrid system with 65% $U_{f.cell}$ (65% $U_{f.stack}$) generated the highest Nernst potential due to higher H_2 partial pressures. In contrast, the recycle hybrid system operating at 65% $U_{f.cell}$ (90% $U_{f.stack}$) produced the lowest potentials. Integrating anode recycle to a hybrid system for 90% $U_{f.stack}$ with the same 65% $U_{f.cell}$ reduced the maximum Nernst potential by 9% (90 mV). This deviation in Nernst potential distribution was mainly driven by the H_2 partial pressure difference because the distributed solid temperature profiles (Fig. 7) for both cases were identical. Both cases at 65% $U_{f.cell}$ were also simulated at similar delta solid temperature, as presented in Table 3.

The resulting electrochemical losses are shown in Fig. 11 to Fig. 13. As expected, the diffusion resistance increased with increasing fuel utilization as the component concentration varied more significantly. The diffusion loss was the least dominant resistance in the system but with the most significant variations among the three case studies.

As shown in Fig. 11, the recycle hybrid system operated at 65% $U_{f.cell}$ (90% $U_{f.stack}$) demonstrated the highest diffusion loss, as opposed to the other two cases without AR. The recirculation of anode-off gas back into the inlet caused significant reduction in the Nernst potential with decreasing H_2 partial pressure. Therefore, the system was required to operate on much higher fuel flow rate intake to gain the same total power from the hybrid system (Table 3). As presented in Fig. 14, operating at 65% $U_{f.cell}$ (90% $U_{f.stack}$) also resulted in the highest H_2O partial pressure, promoting the diffusion resistance in the cell.

As the solid temperature and current density profiles were very similar, 65% $U_{f.cell}$ (65% $U_{f.stack}$) and 65% $U_{f.cell}$ (90% $U_{f.stack}$) did not show significant difference in ohmic and activation losses, as presented in Fig. 12 and Fig. 13. Lower $U_{f.cell}$ brought the system to a lower ohmic and activation resistance in the beginning of the cell and higher at the end of the cell, contradicting the profiles at 90% $U_{f.cell}$.

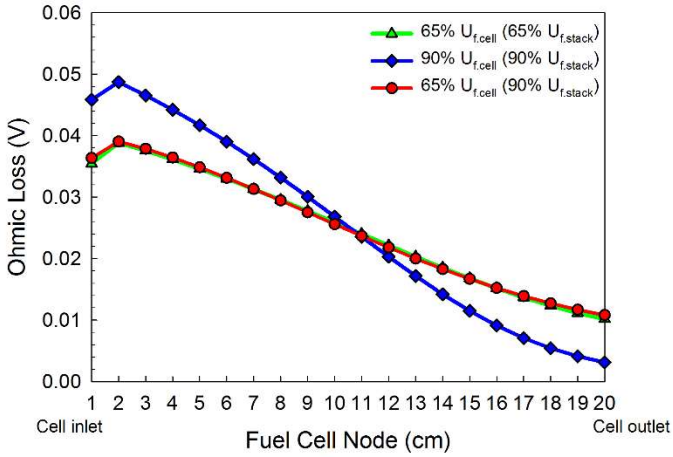

Figure 12: Localized ohmic loss

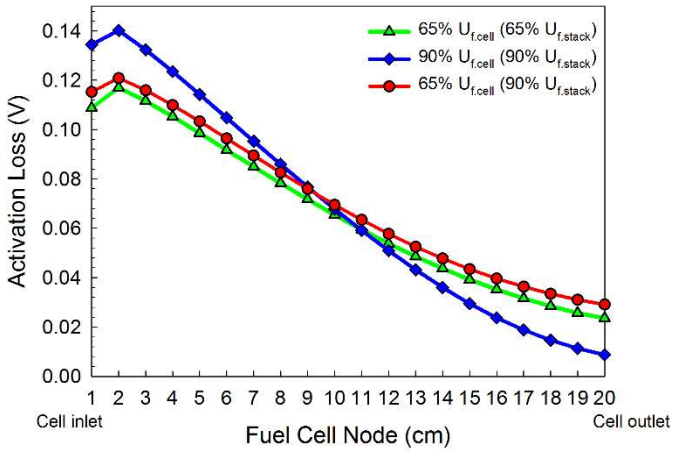

Figure 13: Localized activation loss

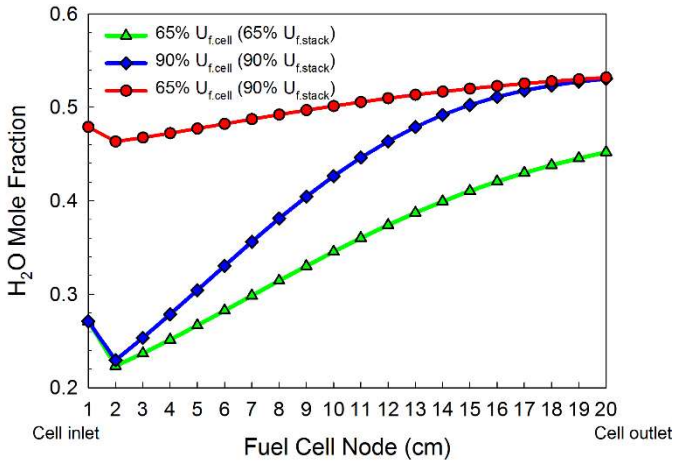

Figure 14: Distributed H_2O mole fraction

The resulting SOFC voltage and the corresponding system performance are presented in Table 5. The efficiency in this work was defined as a ratio of electric power generated by the SOFC and the system based on the lower heating value content (LHV) of the total fuel intake. With the highest Nernst potential at the lowest diffusion resistance, 65% $U_{f.cell}$ (65% $U_{f.stack}$) produced the highest cell voltage. While, the lowest cell voltage was observed in the AR system at 65% $U_{f.cell}$ (90% $U_{f.stack}$) . A 100 mV difference between these two 65% $U_{f.cell}$ cases was strongly attributed to the discrepancy in the Nernst potential or hydrogen partial pressure and the diffusion resistance since activation and ohmic losses were almost identical.

The case of 90% $U_{f.cell}$ (90% $U_{f.stack}$) resulted in the highest stack efficiency (52.6%), as expected, because the stack power generation increased with increasing fuel utilization. Decreasing the fuel utilization from 90% $U_{f.cell}$ to 65% $U_{f.cell}$ in a non recycle hybrid system reduced the stack efficiency to 40%. However, this difference would only bring the total system efficiency down by only 0.4% point, from 71.1% to 70.7%. In terms of the component size requirement, 65% $U_{f.cell}$ required 631,000 less cells in the SOFC stack, but a bigger turbine for additional power of 95 MW, and with approximately 107 kg/s less compressor air intake, as compared to 90% $U_{f.cell}$ (Table 4). Note that the sizing requirement was based on design points for a 550 MW total power production.

Integrating anode recycle for 65% $U_{f.cell}$ (90% $U_{f.stack}$) dramatically reduced the reversible cell voltage, such that reducing the maximum stack efficiency to 36.8%. This efficiency was lower than in 65% $U_{f.cell}$ (65% $U_{f.stack}$) even though both were operated at the same single-pass fuel utilization. The total hybrid efficiency in the AR configuration also decreased by almost 16% point from 90% $U_{f.cell}$ (90% $U_{f.stack}$). As compared to the 90% $U_{f.cell}$ (90% $U_{f.stack}$), the system with AR required a smaller fuel cell size, with about 85,000 less cells, and a relatively larger gas turbine (Table 4).

Table 5 SOFC/GT performance

Fuel Utilization	Voltage (V)	Stack Power (MW)	Stack Efficiency (%)	Total Efficiency (%)
65% $U_{f.cell}$ (65% $U_{f.stack}$)	0.84	311.4	40.0	70.7
90% $U_{f.cell}$ (90% $U_{f.stack}$)	0.79	406.5	52.6	71.1
65% $U_{f.cell}$ (90% $U_{f.stack}$)	0.74	365.0	36.8	55.5

The estimated initial degradation rate in the cell voltage for 1000 hours are shown in Fig. 15. The localized degradation mechanisms were estimated as function of current density, solid temperature, and fuel utilization. The exact same profiles obtained at 65% $U_{f.cell}$ (65% $U_{f.stack}$) and 65% $U_{f.cell}$ (90% $U_{f.stack}$) suggested that the influence of anode recycle on the initial degradation rate at the same single-pass cell fuel utilization was negligible.

The maximum localized degradation was obtained at the beginning of the cell in 90% $U_{f.cell}$ (90% $U_{f.stack}$) . However, this degradation rate reduced by double if operating the system with 65% $U_{f.cell}$ (65% $U_{f.stack}$). Since the temperature profiles in this work were relatively similar for all conditions, the current density as well as the degradation rate variations were strongly driven by fuel utilization. As noticeable in Fig. 15, the first half of the cell length exposed to a higher degradation risk, whereas the second half of the fuel cell length was insensitive to degradation at any fuel utilization as the current density decreased in the maximum solid temperature region.

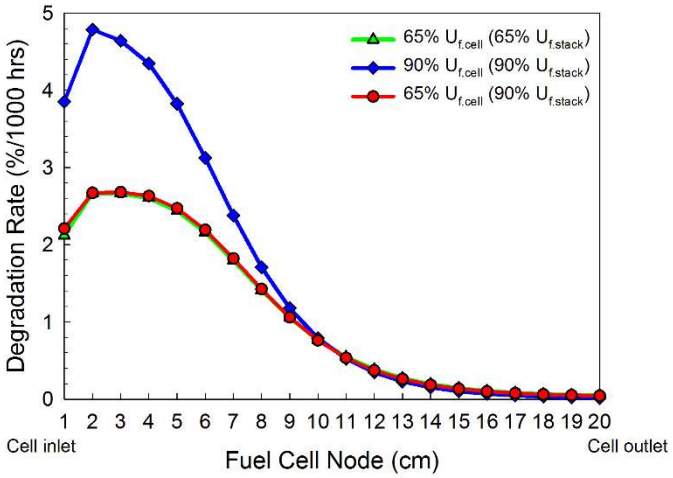

Figure 15: Localized degradation rate

The fuel cell lifetime could be only evaluated in a time-dependent degradation process. The impedance of the cell increased as this region degraded with time. Thus, the maximum current density as shown in Fig. 6 might be shifted toward the cell exit and affected other parameters, which ultimately changing the distribution of localized degradation rate.

CONCLUSIONS

Operating SOFC/GT non-recycle hybrid systems at high fuel utilization using syngas with zero methane does not add significant benefits on total system efficiency. Although lowering fuel utilization from 90% to 65% could reduce stack efficiency by approximately 24%, the total efficiency in a hybrid system without anode recycle decreased by only 0.4% points, from 71.1% to 70.7% (Table 6).

Table 6 Summary of SOFC/GT efficiency analysis

Case	**90% $U_{f.cell}$ (90% $U_{f.stack}$) to 65% $U_{f.cell}$ (65% $U_{f.stack}$)**		**90% $U_{f.cell}$ (90% $U_{f.stack}$) to 65% $U_{f.cell}$ (90% $U_{f.stack}$)**		**65% $U_{f.cell}$ (65% $U_{f.stack}$) to 65% $U_{f.cell}$ (90% $U_{f.stack}$)**	
	%	Impact	%	Impact	%	Impact
Stack efficiency	52.6% to 40.0%	↓ (12.6% point)	52.6% to 36.8%	↓ (15.8% point)	40.0% to 36.8%	↓ (3.2% point)
System efficiency	71.1% to 70.7%	↓ (0.4% point)	71.1% to 55.5%	↓ (15.6% point)	70.7% to 55.5%	↓ (15.2% point)

In fact, lowering fuel utilization from 90% $U_{f.cell}$ to 65% $U_{f.cell}$ in SOFC/GT non-recycle hybrid systems could also reduce the risk of degradation at the beginning of the cell by about half, as a consequence of more evenly distributed performance in the fuel cell system at 65% $U_{f.cell}$. At the same temperature condition, the system demonstrated lower localized current density, lower localized fuel utilization, and relatively lower electrochemical losses, all of which decreased the risk for cell degradation.

It was found that anode recycle caused a dramatic decrease in the total hybrid efficiency at the same stack fuel utilization and the same single-pass cell fuel utilization as in the non-recycle hybrid system. Integrating anode recycle reduced the Nernst potential that contributed to efficiency drop. The fuel cell distributed performance in a hybrid with anode recirculation was more dependent on single-pass cell fuel utilization. Based on the evaluation of initial degradation in this work, anode recycle seemed insensitive in determining the fuel cell degradation. However, this might be different if the dynamic degradation and impurities effects were considered.

DISCLAIMER

ACKNOWLEDGMENT

This work was funded by the U.S Department of Energy Crosscutting Research program, implemented through the Technology Development & Integration Center, Coal, in The Office of Fossil Energy.

NOMENCLATURE

AR	Anode recycle/recirculation
SOFC	Solid oxide fuel cell
GT	Gas turbine
IEA	International Energy Agency
LHV	Low-heating value
ASR	area specific resistance [Ω-m^2]
V_{cell}	Cell voltage, overpotential [V]
V_{Nernst}	Nernst potential [V]
$\Delta G^{\circ}_{H_2O}$	Standard Gibbs free energy [kJ]
α	charge transfer coefficient
F	Faraday's constant [C/mol]
i	current density [A/cm^2]
i_0	exchange current density [A/cm^2]
K_p	equilibrium constant
n	number of electrons transfer per reaction
η	electrochemical loss [V]
p	Partial pressure [atm]

R_u	Ideal gas constant [J/mol-K]
r_d	degradation rate [%/1000hr]
T	Temperature [K]
TPB	triple phase boundary
U_f	fuel utilization
WGS	Water-gas shift
x	mole fraction
bulk	anode/cathode stream
act	activation
dif	diffusion
ohm	ohmic

REFERENCES

[1] Tarroja, B., Mueller, F., Maclay, J., and Brouwer, J., 2010, "Parametric thermodynamic analysis of a solid oxide fuel cell gas turbine system design space," Journal of Engineering for Gas Turbines and Power, 132(7), pp. 072301-072301.

[2] Borji, M., Atashkari, K., Nariman-zadeh, N., and Masoumpour, M., 2015, "Modeling, parametric analysis and optimization of an anode-supported planar solid oxide fuel cell," Proceedings of the Institution of Mechanical Engineers, Part C: Journal of Mechanical Engineering Science, 229(17), pp. 3125-3140.

[3] Uechi, H., Kimijima, S., and Kasagi, N., 2004, "Cycle analysis of gas turbine–fuel cell cycle hybrid micro generation system," Journal of Engineering for Gas Turbines and Power, 126(4), pp. 755-762.

[4] Santarelli, M., Leone, P., Calì, M., and Orsello, G., 2007, "Experimental evaluation of the sensitivity to fuel utilization and air management on a 100 kW SOFC system," Journal of Power Sources, 171(1), pp. 155-168.

[5] Calise, F., Restucccia, G., and Sammes, N., 2010, "Experimental analysis of micro-tubular solid oxide fuel cell fed by hydrogen," Journal of Power Sources, 195(4), pp. 1163-1170.

[6] Tanaka, Y., Terayama, T., Momma, A., and Kato, T., 2015, "Numerical simulation of SOFC system performance at 90% fuel utilization with or without anode off-gas recycle for enhancing efficiency," ECS Transactions, 68(1), pp. 293-300.

[7] Gemmen, R. S., and Johnson, C. D., 2006, "Evaluation of fuel cell system efficiency and degradation at development and during commercialization," Journal of Power Sources, 159(1), pp. 646-655.

[8] Barelli, L., Barluzzi, E., and Bidini, G., 2013, "Diagnosis methodology and technique for solid oxide fuel cells: A review," International Journal of Hydrogen Energy, 38(12), pp. 5060-5074.

[9] Tu, H., and Stimming, U., 2004, "Advances, aging mechanisms and lifetime in solid-oxide fuel cells," Journal of Power Sources, 127(1–2), pp. 284-293.

[10] Nehter, P., 2007, "A high fuel utilizing solid oxide fuel cell cycle with regard to the formation of nickel oxide and power density," Journal of Power Sources, 164(1), pp. 252-259.

[11] McIntosh, S., and Gorte, R. J., 2004, "Direct hydrocarbon solid oxide fuel cells," Chemical Reviews, 104(10), pp. 4845-4866.

[12] Tucker, D., Abreu-Sepulveda, M., and Harun, N. F., 2014, "SOFC lifetime assessment in gas turbine hybrid power systems," Journal of Fuel Cell Science and Technology, 11(5), pp. 1-7.

[13] Noponen, M., Halinen, M., Saarinen, J., and Kiviaho, J., 2007, "Experimental study of anode gas recycling on efficiency of SOFC," ECS Transactions, 5(1), pp. 545-551.

[14] Tanaka, Y., Momma, A., Sato, K., and Kato, T., 2011, "Improvement of electrical efficiency of solid oxide fuel cells by anode gas recycle," ECS Transactions, 30(1), pp. 145-150.

[15] Peters, R., Deja, R., Blum, L., Pennanen, J., Kiviaho, J., and Hakala, T., 2013, "Analysis of solid oxide fuel cell system concepts with anode recycling," International Journal of Hydrogen Energy, 38(16), pp. 6809-6820.

[16] Baba, S., Kobayashi, N., Takahashi, S., and Hirano, S., 2014, "Development of anode gas recycle system using ejector for 1 kw solid oxide fuel cell," Journal of Engineering for Gas Turbines and Power, 137(2), pp. 021504-021504.

[17] Winkler, W., Nehter, P., Williams, M. C., Tucker, D., and Gemmen, R., 2006, "General fuel cell hybrid synergies and hybrid system testing status," Journal of Power Sources, 159(1), pp. 656-666.

[18] Haynes, C., and Wepfer, W. J., 2000, "'Design for Power' of a commercial grade tubular solid oxide fuel cell," Energy Conversion and Management, 41(11), pp. 1123-1139.

[19] Zhao, Y., Sadhukhan, J., Lanzini, A., Brandon, N., and Shah, N., 2011, "Optimal integration strategies for a syngas fuelled SOFC and gas turbine hybrid," Journal of Power Sources, 196(22), pp. 9516-9527.

[20] Buonomano, A., Calise, F., d'Accadia, M. D., Palombo, A., and Vicidomini, M., 2015, "Hybrid solid oxide fuel cells–gas turbine systems for combined heat and power: A review," Applied Energy, 156, pp. 32-85.

[21] Bakalis, D. P., and Stamatis, A. G., 2014, "Optimization methodology of turbomachines for hybrid SOFC–GT applications," Energy, 70, pp. 86-94.

[22] Gandiglio, M., Lanzini, A., Leone, P., Santarelli, M., and Borchiellini, R., 2013, "Thermoeconomic analysis of large solid oxide fuel cell plants: Atmospheric vs. pressurized performance," Energy, 55, pp. 142-155.

[23] Stiller, C., Thorud, B., Bolland, O., Kandepu, R., and Imsland, L., 2006, "Control strategy for a solid oxide fuel cell and gas turbine hybrid system," Journal of Power Sources, 158(1), pp. 303-315.

[24] Jiang, W., Fang, R., Khan, J., and Dougal, R., 2009, "Control strategies for start-up and part-load operation of solid oxide fuel cell/gas turbine hybrid system," Journal of Fuel Cell Science and Technology, 7(1), pp. 011016-011016.

[25] Yi, Y., Rao, A. D., Brouwer, J., and Samuelsen, G. S., 2004, "Analysis and optimization of a solid oxide fuel cell and intercooled gas turbine (SOFC–ICGT) hybrid cycle," Journal of Power Sources, 132(1–2), pp. 77-85.
[26] Park, S. K., Ahn, J.-H., and Kim, T. S., 2011, "Performance evaluation of integrated gasification solid oxide fuel cell/gas turbine systems including carbon dioxide capture," Applied Energy, 88(9), pp. 2976-2987.
[27] Trembly, J. P., Gemmen, R. S., and Bayless, D. J., 2007, "The effect of coal syngas containing ash3 on the performance of SOFCs: Investigations into the effect of operational temperature, current density and AsH3 concentration," Journal of Power Sources, 171(2), pp. 818-825.
[28] Hughes, D., Wepfer, W. J., Davies, K., Ford, J. C., Haynes, C., and Tucker, D., "A real-time spatial SOFC model for hardware-based simulation of hybrid systems," Proc. ASME 2011 9th International Conference on Fuel Cell Science, Engineering and Technology collocated with ASME 2011 5th International Conference on Energy Sustainability, pp. 409-428.
[29] Li, M., Powers, J. D., and Brouwer, J., 2010, "A finite volume SOFC model for coal-based integrated gasification fuel cell systems analysis," Journal of Fuel Cell Science and Technology, 7(4), pp. 041017-041017.
[30] Achenbach, E., 1996, "SOFC stack modeling, final report of activity A2, Annex II: Modeling and evaluation of advanced solid oxide fuel cells, International Energy Agency Programme on R, D&D on Advanced Fuel Cells," International Energy Agency, Juelich, Germany.
[31] Tucker, D., Pezzini, P., and Banta, L., 2013, "Equivalence ratio startup control of a fuel cell turbine hybrid system," ASME Turbo Expo 2013: Power for Land, Sea and AirSan Antonio, Texas, USA, p. 11.
[32] Zhou, N., Yang, C., and Tucker, D., 2015, "Evaluation of cathode air flow transients in a SOFC/GT Hybrid System Using Hardware in the Loop Simulation," Journal of Fuel Cell Science and Technology, 12(1), pp. 011003-011003.
[33] Zaccaria, V., Tucker, D., and Traverso, A., 2016, "Transfer function development for SOFC/GT hybrid systems control using cold air bypass," Applied Energy, 165, pp. 695-706.
[34] Harun, N. F., Tucker, D., and Adams Ii, T. A., 2016, "Impact of fuel composition transients on SOFC performance in gas turbine hybrid systems," Applied Energy, 164, pp. 446-461.
[35] Zaccaria, V., Tucker, D., and Traverso, A., 2016, "A distributed real-time model of degradation in a solid oxide fuel cell, part I: Model characterization," Journal of Power Sources, 311, pp. 175-181.